— 修士論文—

Study on Dual Circular Polarization Antenna System with Improved Off-axis XPD for Small Satellite Downlink Communication

（小型衛星両円偏波ダウンリンク通信用アンテナシステム偏軸交差偏波識別度を改善ための研究）

平成 30 年 7 月提出

指導教員: 齋藤宏文教授

電気系工学専攻
37-165062 王天宇

Contents

1. Introduction

1.1 Research Background

Small satellite missions play a key and attractive role in various scientific and engineering programs. They have been responsible for greatly reducing the time to obtain science and technology results. Small satellite missions tend to be flexible and can thereby be extremely responsive to new opportunities or technological needs. The shorter development periods for small missions can reduce overall costs and can thus provide welcome budgetary options for highly constrained space programs. Recently the technology for small satellites has been developed rapidly and many earth observation missions are proposed [1]. Fig.1.1 shows the 50kg small scientific satellite “INDEX” (REIMEI) for aurora observations and demonstrations of advanced satellite technologies launched in 2005. Fig. 1.2 shows the 260kg light weight Synthetic Aperture Radar (SAR) satellite TecSAR launched in 2008.

High-bit-rate communication system is needed due to large quantities of data generated by high-resolution sensors and has to be transmitted quickly to ground station. Compared to large satellites, downlink capability is one of the main limitations of small satellites due to their limited mass requirement and power resources. Onboard instruments must be light-weighted and low-power consumed but with high performance.

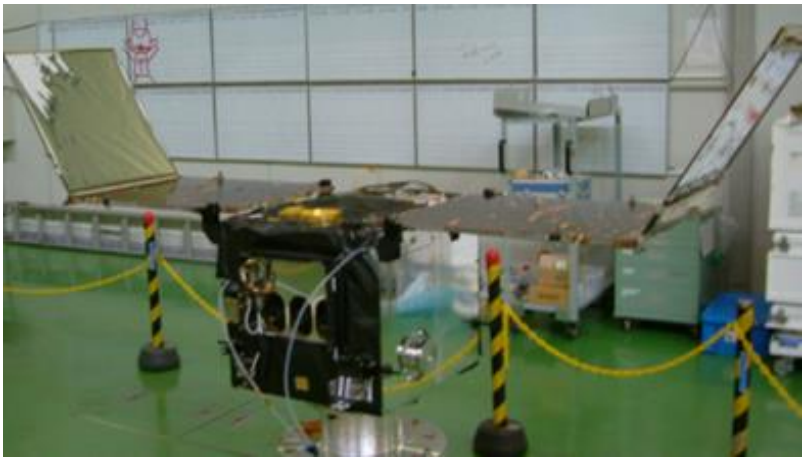

Fig.1.1 REIMEI Satellite

Fig.1.2 TecSAR Satellite

1.2 Research Purpose

Small satellite downlink communication speed has been increased in the past years. Small earth observation satellite, Skysat has achieved 303 Mbps downlink by 8PSK modulation [2]. Our lab achieved 505 Mbps downlink on 66kg satellite Hodoyoshi 4 by right-hand circular polarization (RHCP) operation [3]. We plan to realize a 2Gbps class ultrahigh speed data communication in X band (8025MHz-8400MHz) on a 100kg small satellite by using both RHCP and left-hand circular polarization (LHCP) channels simultaneously. Communication systems operating with circular polarization (CP) have intrinsic advantages in comparison with that using linear polarization (LP). In comparison to LP, CP eliminates Faraday rotation effect during signal propagation, and also avoids the need of alignment between satellite and ground station terminal antennas [4]. Utilizing two orthogonal channels allows a more efficient utilization of the electromagnetic spectrum and increases the link capacity. The communication speed becomes double compared to present system using only one channel. An important requirement in such a system is the high cross-polarization discrimination (XPD) to prevent interference between signals carried by orthogonal circular polarization carriers.

Many researches have been focused on high XPD antenna design including microstrip antenna, multimode horn, etc. Some satellite onboard antenna system design methodology for dual circular polarization

communication has been introduced by researchers [5][6]. Antenna systems include a septum polarizer and a corrugated horn seems the best choice due to its great on-axis XPD performance. However, it still shows relatively not good XPD performance off-axis due to the narrow angle cross-polarization pattern characteristic of the conventional conical corrugated horn antenna. Sum of the desired polarization and cross polarization is an elliptic polarization. In practical, on-board antenna has limited adjustment ability and it cannot be guaranteed pointing to the ground antenna exactly, thus the ground antenna receives elliptical polarized wave which has high level cross-polarization components. This means there will be high level cross-talk between two orthogonal channels.

We focus on onboard system contain a polarizer and a horn antenna. This research derives the appropriate horn antenna aperture field distribution from desirable radiation pattern. General electromagnetic analysis of hybrid mode waveguide (horn) are given to achieve desired aperture field pattern, which could give a guidance to antenna design. The final goal is to design an onboard antenna system with improved off-axis XPD performance.

1.3 Paper Organization

This paper has six chapters:

Chapter 1 introduces the research background and research purposes of this paper;

Chapter 2 introduces the most important concept XPD and shows the importance of the research. Outline of the antenna system is given in this chapter;

Chapter 3 is the core of this paper. The appropriate antenna aperture field distribution is desired from desirable radiation pattern. Then general modal analysis of circular waveguide with constant impedance anisotropic boundary which could support hybrid mode wave are given. It shows under balanced hybrid boundary condition, the aperture transverse E field of fundamental HE_{11} mode can achieve desired linear shape and circularly symmetrical pattern for high XPD communication.

Chapter 4 introduces corrugated surface as a realization of desired boundary stated in Chapter 3. A design methodology of corrugated conical horn antenna and simulation results are also given.

Chapter 5 introduces corrugated gaussian profiled horn antenna which aim to further improve XPD performance of conventional corrugated horn. Design and simulation results are also given.

Chapter 6 is summary of the research.

2. Onboard Antenna System

2.1 Definition of XPD

2.1.1 Polarization

Consider a wave traveling in z direction which both E_x and E_y exist,

$$\boldsymbol{E} = (\boldsymbol{u}_x A + \boldsymbol{u}_y B)\, e^{-jkz} \tag{2.1}$$

where A and B are amplitudes of the electric field in x and y direction, respectively. $\boldsymbol{u}_x$ and $\boldsymbol{u}_y$ are unit vectors. Wave number is defined as $k = 2\pi / \lambda$. If $B = 0$, the wave is LP wave in the x direction. If $A = 0$, the wave is LP wave in the y direction. If A and B are both real (or complex with equal phases), we again have a LP wave, with the axis of polarization inclined at an angle *arctan*(B/A) with respect to the x axis. If A and B are complex with different phase angles, $\boldsymbol{E}$ (instantaneous electric intensity) will no longer point in a single spatial direction. Letting $A = |A| e^{ja}$ and $B = |B| e^{jb}$, then we have

$$\begin{aligned} E_x &= \sqrt{2}\,|A|\, cos(\omega t - kz + a) \\ E_y &= \sqrt{2}\,|\mathrm{B}|\, cos(\omega t - kz + b) \end{aligned} \tag{2.2}$$

If $|A| = |B|$, $a\text{-}b = 90^\circ$, then $|\boldsymbol{E}|^2 = 2|A|^2 = \text{const}$. It can be easily seen that the tip of electric field vector traces out a circular locus in x-y plane, and the vector has a clockwise sense of rotation when it is viewed along z axis. Then this wave is said to have RHCP (Fig.2.1b). If we change $a\text{-}b = -90^\circ$, the electric field vector will have a counterclockwise sense of rotation and the polarization is designated as LHCP (Fig.2.1a). So circular polarized wave

can be achieved by two orthogonal LP wave have equal amplitudes and a 90° phase difference of one relative to another. This is the principle of polarizer to obtain CP wave. When $|A| = |B|$ but $a\text{-}b \neq 90^\circ$, the tip of vector traces out an ellipse and the field is said to be elliptically polarized. LP and CP are both special cases of elliptical polarization. Axial ratio (AR), which is the ratio of the magnitudes of the major and minor axis defined by the electric field vector, is an important parameter to judge the circularity of CP.

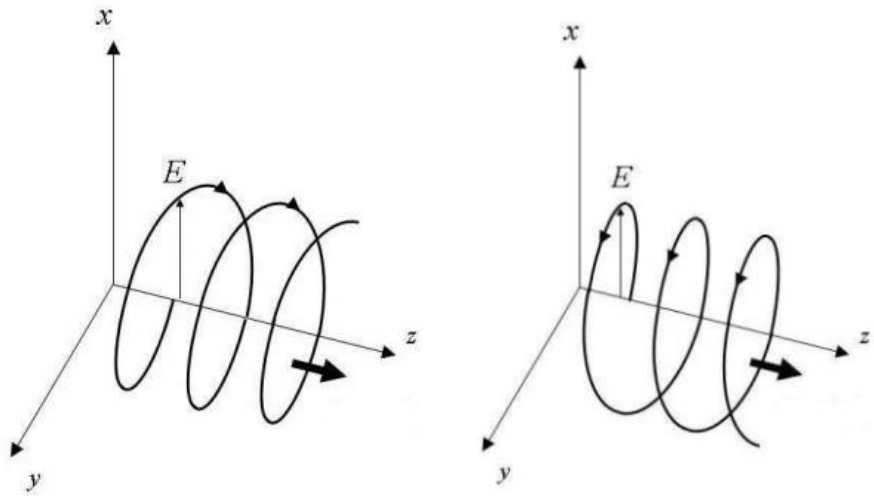

(a) LHCP wave (b) RHCP wave

Fig.2.1. CP polarization wave

2.1.2 Cross Polarization and XPD

An elliptical polarized wave can be decomposed into *x* and *y* direction linearly polarized waves. In general, any two orthogonal waves can be used as basis to represent an arbitrarily polarized wave. Thus, theoretically we could use any two orthogonal channels to transmit signals. In our case we use RHCP and LHCP channels.

While propagating from satellite to an earth station, a main polarization

wave may be converted to another polarization as shown in Fig.2.2. For example, assume pure RHCP signal is transmitted, but antenna at the receiving terminal still would receive some undesired LHCP signal. The desired and undesired field components are called as co-polarized and cross-polarized field, respectively. XPD is an important parameter to describe this cross-talk effect. It is defined as ratio of the co-polarized component of the specified polarization compared to the orthogonal cross-polar component.

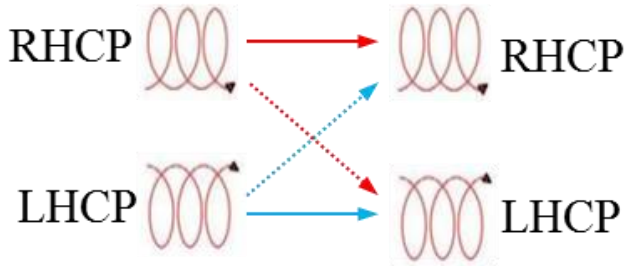

Fig.2.2 Cross-talk effect in two orthogonal channels

2.2 Onboard Antenna System

We use 64APSK modulation scheme in our communication system. For achieving low bit rate error communication, the XPD requirement for antenna system is stringent: XPD>40dB [3]. In our design, we focus on antenna system contains a septum polarizer and a horn antenna, as illustrated in Fig.2.3. TE_{10} mode linearly polarized signals (dominant mode in rectangular waveguide) propagate into the polarizer from two ports and generate high purity RHCP and LHCP signals at output simultaneously. Signals transmit into the corrugated horn antenna and radiate to free space. On-axis XPD is mainly dependent on the polarizer while off-axis XPD

performance is mainly dependent on horn antenna.

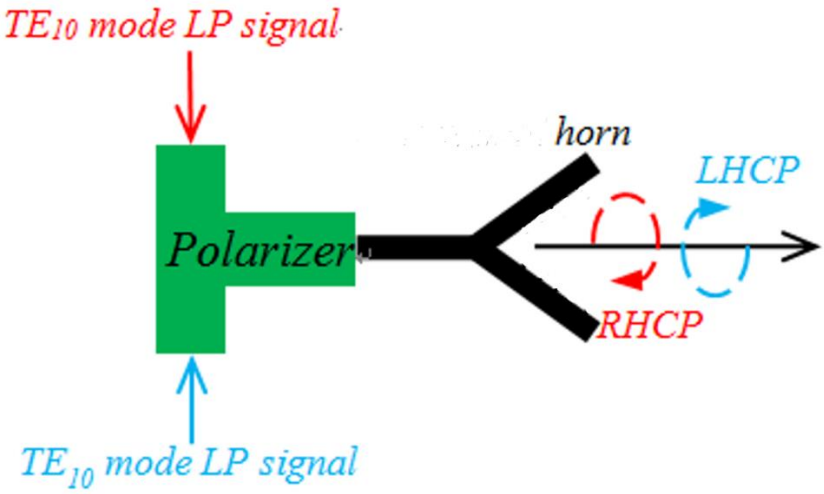

Fig.2.3 Onboard antenna system

2.3 Stepped-septum Polarizer

2.3.1 Principle of Polarizer

Stepped-septum polarizer shown in Fig.2.4, which can be modeled as several short-length ridged waveguide with different ridge height cascade progressively, was proposed by M.H. Chen and G.N. Tsandoulasp [7]. The basic principle can be explained by even and odd mode excitation illustrated in Fig.2.4 (a) (b). Even mode excitation wave (equally amplitudes with same direction TE_{10} modes excitation of two input ports) remains TE_{10} mode in the output square waveguide. However, even mode (equally amplitudes with opposite direction TE_{10} modes excitation of two input ports) excitation will cause mode coupling, reflection and phase change. With proper septum design, even mode waves will mostly converted to TE_{10} mode in the output and achieve desired 90° phase change. From Fig.2.4 (c) (d), it shows the excitation of each port is a superposition even and odd excitation, thus RHCP and LHCP waves generates in the output.

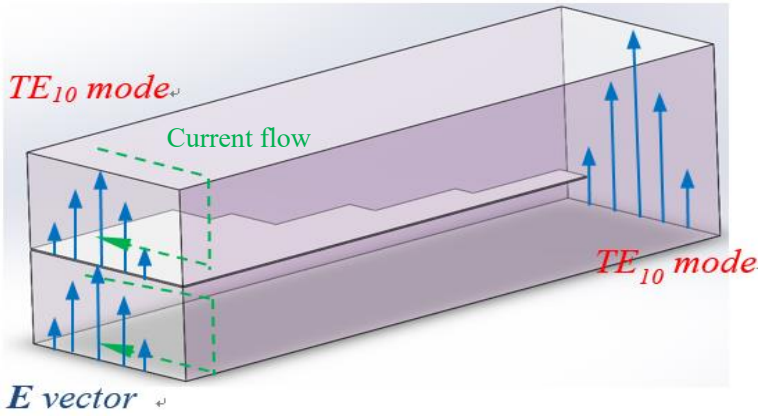
TE10 mode
Current flow
TE10 mode
E vector

(a)

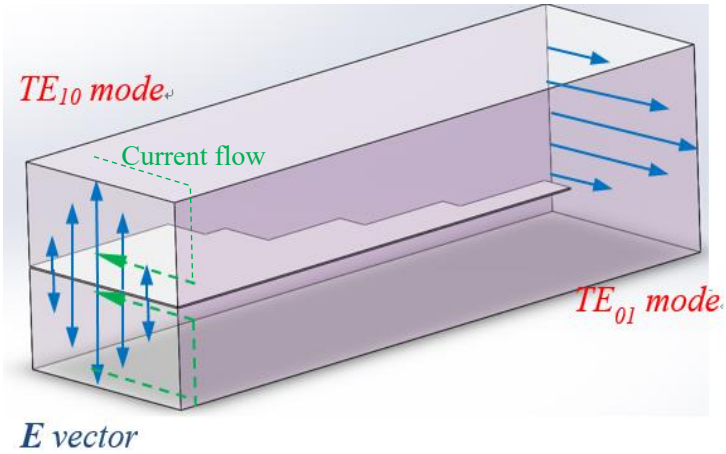
TE10 mode
Current flow
TE01 mode
E vector

(b)

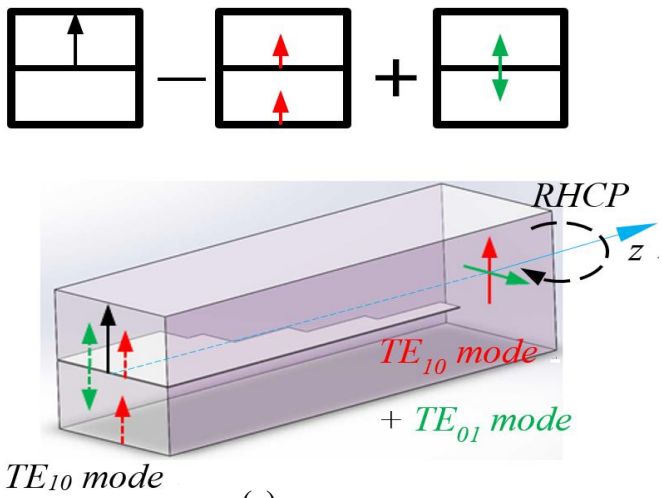
RHCP
z
TE10 mode
+ TE01 mode
TE10 mode

(c)

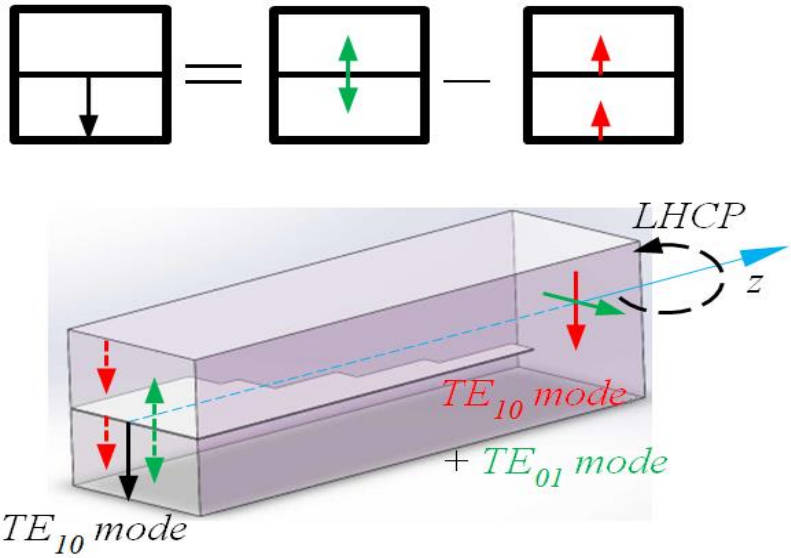

(d)

Fig.2.4. Septum polarizer (a) Even mode (b) Odd mode (c) RHCP excitation (d) LHCP excitation

2.3.2 Design and Simulation of Polarizer

Polarizer is operating in X-band so standard WR90 input waveguide is chosen. Phase change is mainly determined by septum partition length while reflection is suppressed by choosing septum partition height properly. We first choose initial septum size by considering dominant mode wave's propagation and using transvers resonant method. It shows good agreement with sizes obtained by CHEN's strategy [7]. Then we use finite-element method HFSS to optimize XPD.

We head-to-head concatenate two polarizers to from a 4-port network for calculating S parameters. As stated before, XPD requirement for the polarizer is XPD>40dB. For port 1 excitation, these S parameters have the following physical meaning [8] and are used to evaluate performance of

polarizer: S_{11}—reflection (S_{11}<-40 dB required); S_{21}—isolation (S_{21}<-30 dB required); S_{31}—insertion (S_{31}>-0.1 dB required); S_{41}—cross polarization (S_{41}<-30 dB required). Simulation model and results are shown in Fig.2.5, 2.6, respectively. It shows that polarizer meets the requirement in 8.0-8.4GHz. Especially it shows S_{41} achieves -50dB at center frequency which indicate good XPD performance.

The rest part of this paper will handle horn antenna which highly influence off-axis XPD performance.

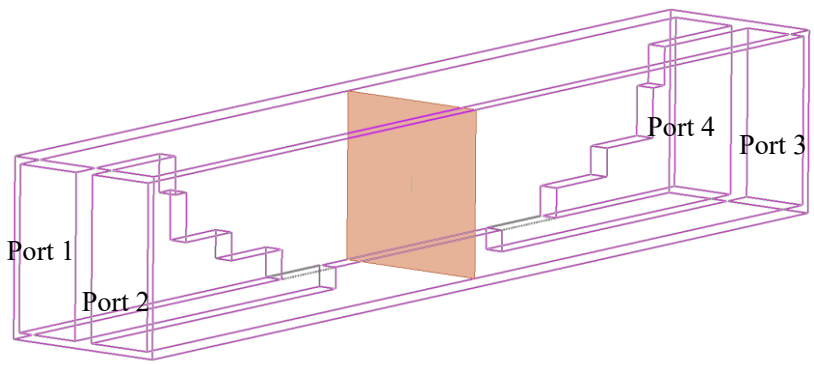

Fig.2.7. Simulation model for calculating S parameters

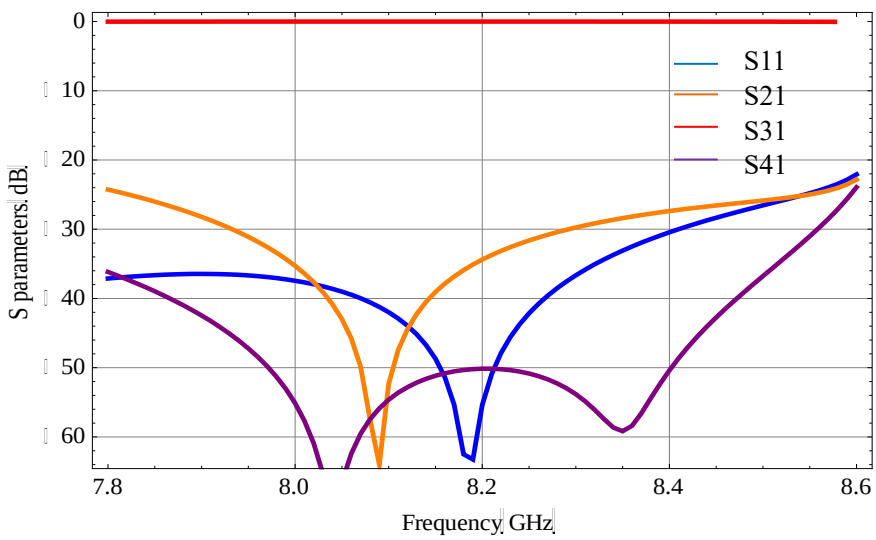

Fig.2.8. S parameters versus frequency in model

3. Theory of Hybrid Mode Waveguide

Aperture antenna (waveguide or horn) is essential for radiating low cross-polarization waves. It is reasonable that specific aperture field pattern is necessary to fulfill this goal. In Part 3.1, CP problem is converted to LP problem. It will be shown that the requirement to produce a low crosspolar level radiated field can only be met by a circular aperture with linearly and circular symmetric distributed aperture electric field under LP operation.

Conventional circular isotropic smooth metallic waveguide can only support pure transverse electric (TE) or transverse magnetic (TM) modes where their aperture transverse field lines are curved. Waveguides or horns with anisotropic walls which have appropriate surface impedances could excite hybrid modes which is the combination of TE and TM modes. These hybrid modes give a possibility to produce desired linear and rotational symmetric aperture field in Part 3.2. Various artificial anisotropic walls are investigated and already used in waveguides or horns in different applications: transversely corrugated surfaces [9], longitudinal corrugated surfaces [10], strip-loaded surfaces [11] and metamaterial surfaces [12] [13]. Hence, we give a general modal analysis of circular waveguide with constant anisotropic surface in Part 3.3. Surface impedances on waveguide boundary are defined as boundary conditions. Hybrid HE and EH modes are then expanded analytically in this hybrid mode circular waveguide by solving the boundary-value problem. Dispersion equation and exact expressions of

electric and magnetic fields are derived. It will be shown that when surface impedances satisfy specific condition known as balanced hybrid condition [14], fundamental HE_{11} mode can achieve desired aperture pattern for high XPD communication.

3.1 Conditions for Aperture Field Distribution to Achieve High XPD Dual CP Communication

3.1.1 Principle of High XPD Aperture Radiation

Our attention is focused on uniform circular waveguides and conical horns with circular aperture. ω is supposed to be the wave angular temporal frequency. When antenna operates under LP operation, the transverse electric field in the aperture is assumed, such as that of Fig.3.1(a). The radiated field in the far field region from aperture has only θ and ϕ components.

Without loss of generality, antenna under LHCP operation is considered. The LP aperture field distribution would rotate clockwise with angular frequency ω around central axis as shown in Fig.3.1(b), which causes LP radiation field distribution rotates with same angular frequency. Fig.3.2 gives how radiated field behaves under LHCP operation. Consider arbitrary chosen P and P' on $\phi=0$ and $\phi=\phi_0$ planes with same polar angle θ, respectively. Assume radiated fields on P and P' at t=0 are

$$\boldsymbol{E}_P(t=0) = E_P \cos\alpha_0 \boldsymbol{e}_\theta + E_P \sin\alpha_0 \boldsymbol{e}_\phi \tag{3.1}$$

$$\boldsymbol{E}_{P'}(t=0) = E_{P'} \cos\alpha_1 \boldsymbol{e}_\theta + E_{P'} \sin\alpha_1 \boldsymbol{e}_\phi \tag{3.2}$$

where α_i (i=0,1) are inclination angles, $E_{p'}$ and $E_{p'}$ are amplitudes. After time interval $t_0 = \phi_0/\omega$, LP field distribution rotates around z axis $\omega t_0 = \phi_0$ clockwise, which means $\phi = \phi_0$ plane field pattern at t=0 rotates ϕ_0 and coincide with ϕ=0 plane field pattern at $t=t_0$. Therefore, the electric field of P at $t=t_0$ has the same orientation on $\theta\ \phi$-plane and amplitude as that of P' at t=0,

$$\boldsymbol{E}_P(t=t_0) = E_{P'}\cos\alpha_1\boldsymbol{e}_\theta + E_{P'}\sin\alpha_1\boldsymbol{e}_\phi \tag{3.3}$$

In high XPD communication, it is expected that radiated field is purely LHCP if antenna is under LHCP operation, i.e. field vector rotates clockwise on $\theta\ \phi$-plane with constant amplitude and angular frequency ω. Therefore,

$$\begin{aligned}\boldsymbol{E}_P(t=t_0) &= E_P\cos(\alpha_0-\omega t_0)\boldsymbol{e}_\theta + E_P\sin(\alpha_0-\omega t_0)\boldsymbol{e}_\phi \\ &= E_P\cos(\alpha_0-\phi_0)\boldsymbol{e}_\theta + E_P\sin(\alpha_0-\phi_0)\boldsymbol{e}_\phi\end{aligned} \tag{3.4}$$

From (3.2)-(3.4),

$$\boldsymbol{E}_{P'}(t=0) = E_P\cos(\phi_0-\alpha_0)\boldsymbol{e}_\theta - E_P\sin(\phi_0-\alpha_0)\boldsymbol{e}_\phi \tag{3.5}$$

which means $\boldsymbol{E}_P$ and $\boldsymbol{E}_{P'}$ have identical amplitude. Due to the arbitrariness of P and P', the necessary and sufficient condition for zero cross polarization CP communication is deduced: under LP operation, radiated field components have the form

$$\boldsymbol{E}_\theta(\theta,\phi) = E(\theta)\cos(\phi-\alpha)\boldsymbol{e}_\theta - E(\theta)(\phi-\alpha)\boldsymbol{e}_\phi \tag{3.6}$$

where α is an arbitrary angle. Therefore, an antenna under LP operation satisfies conditions:

(i) have identical ϕ-plane amplitude and phase patterns;

(ii) oriented along the unit vector $\boldsymbol{i}$=cos(ϕ-α)$\boldsymbol{e}_\theta$ - sin(ϕ-α)$\boldsymbol{e}_\phi$,

would have zero cross polarization under CP operation. In the follow part of this chapter, it is enough to focus our attention on LP operation.

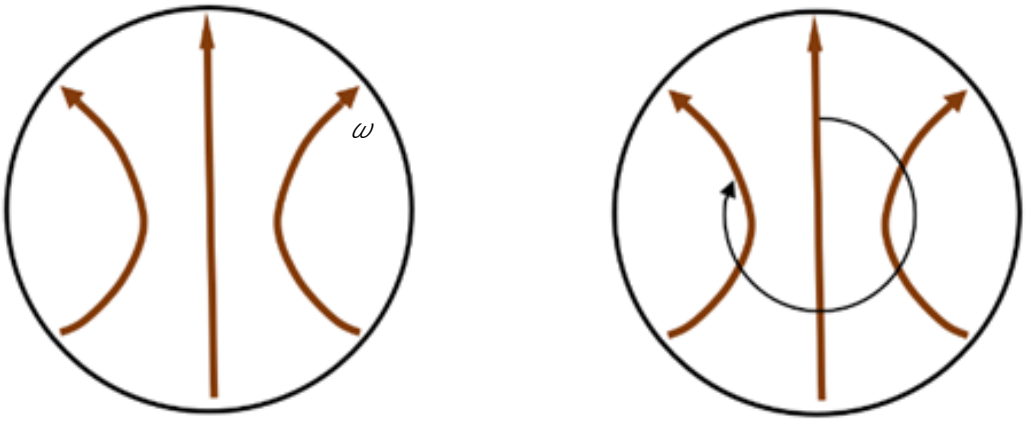

(a) LP operation (b) CP operation

Fig.3.1. Illustration of aperture transverse electric field configuration of waveguides (horn)

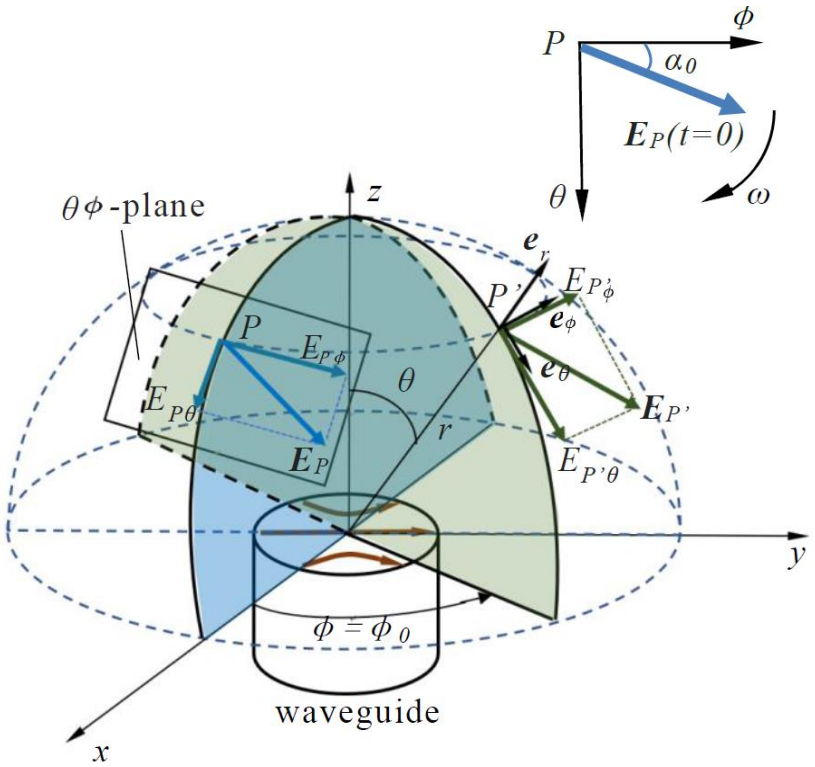

(a) t=0

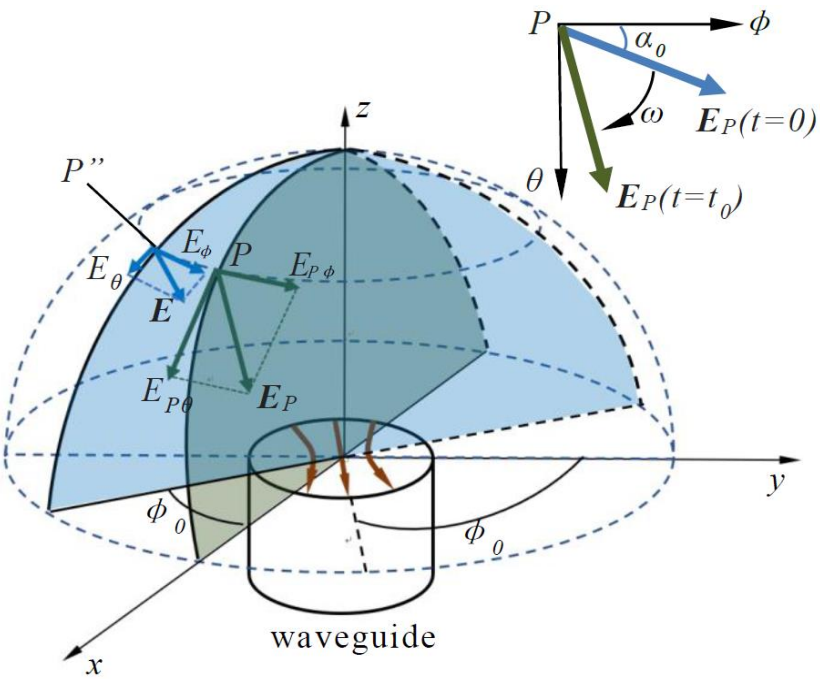

(b) t=t_0

Fig.3.2. Illustration of aperture field radiation under LHCP operation

3.1.2 Aperture Field Pattern Condition

Assume $\boldsymbol{E_a}$ and $\boldsymbol{H_a}$ are tangential aperture fields on aperture A. The Fourier transforms of aperture fields are defined as

$$\begin{aligned} \boldsymbol{P} &= \int_A \boldsymbol{E}_a(\boldsymbol{r}')e^{j\boldsymbol{k}\cdot\boldsymbol{r}'}dS' = P_x\boldsymbol{e}_x + P_y\boldsymbol{e}_y \\ \boldsymbol{Q} &= \int_A \boldsymbol{H}_a(\boldsymbol{r}')e^{j\boldsymbol{k}\cdot\boldsymbol{r}'}dS' = Q_x\boldsymbol{e}_x + Q_y\boldsymbol{e}_y \end{aligned} \tag{3.7}$$

where $\boldsymbol{k}$ is the wavenumber vector. According to field equivalence principle, the radiated field is related to the Fourier transforms of aperture fields [15] by

$$\begin{aligned} \boldsymbol{E}_\theta &= \frac{jk_0}{4\pi r}e^{-jk_0 r}(1+\cos\theta)[P_x\cos\phi + P_y\sin\phi] \\ \boldsymbol{E}_\phi &= \frac{jk_0}{4\pi r}e^{-jk_0 r}(1+\cos\theta)[P_y\cos\phi - P_x\sin\phi] \end{aligned} \tag{3.8}$$

when the transverse aperture fields satisfy Huygens source condition

$$\boldsymbol{e}_z \times \boldsymbol{E}_a = \eta_0 \boldsymbol{H}_a \tag{3.9}$$

k_0 and η_0 represent wavenumber and wave impedance in free space, respectively.

From (3.7)-(3.8), condition (i) (ii) in Part 3.1.1 is satisfied with α=0 when aperture field satisfies:

(i') aperture field is purely linear, i.e. E_y=0;

(ii') aperture field is circular symmetric distributed, i.e. E_{ax} is ϕ independent.

(iii') transverse aperture fields satisfy Huygens source condition

3.2 Hybrid Mode Waveguide

Hybrid mode waveguide with anisotropic wall in cylindrical system oriented in z direction is shown in Fig.3.3.

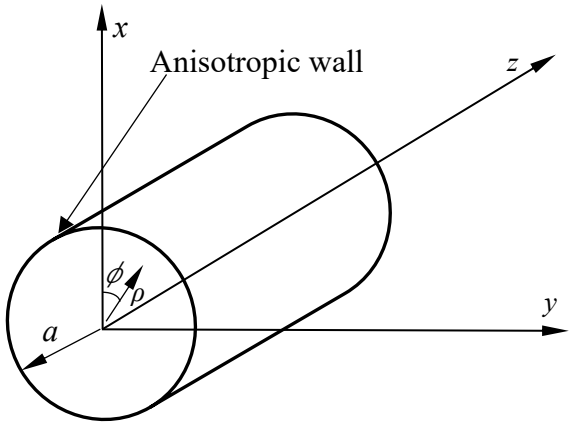

Fig.3.3. Hybrid mode waveguide with anisotropic wall

3.2.1 Surface Impedance Definition and Boundary Condition

Surface impedances at boundary wall ($\rho=a$) are defined as

$$Z_\phi = -\frac{E_\phi}{H_z}\Big|_{\rho=a}, \qquad Z_z = \frac{E_z}{H_\phi}\Big|_{\rho=a} \tag{3.10}$$

Waveguides considered in the following is assumed to have constant surface impedances for all plane waves with different incident angles or transverse wavenumbers. Hence (3.10) can also treated as boundary condition expression.

3.2.2 Electromagnetic Fields Expression for Hybrid Modes

All fields considered later are:

(1) time harmonic with factor $e^{j\omega t}$;

(2) propagate in z direction and have z-dependence factor $e^{-j\beta z}$,

where β is the propagation wavenumber along z axis. These two factors will be further omitted.

Assume waveguide supports hybrid mode which is combination of TM and TE modes. Longitudinal fields E_z and H_z satisfy Helmholtz equation and has expressions,

$$E_z = A_m J_m(k_c\rho)\begin{Bmatrix}\cos(m\phi)\\ \sin(m\phi)\end{Bmatrix}$$
$$\eta_0 H_z = B_m J_m(k_c\rho)\begin{Bmatrix}\sin(m\phi)\\ -\cos(m\phi)\end{Bmatrix} \tag{3.11}$$

where k_c is the cutoff wavenumber, $\eta_0=(\mu_0/\varepsilon_0)^{1/2}$ is the free space wave impedance, ε_0 and μ_0 are the permittivity and permeability of vacuum, $J_m(\cdot)$ is the Bessel function of the first kind and order m, m is positive constant number, A_m and B_m are amplitudes. Then transverse fields components can be deduced by E_z and H_z [15],

$$\boldsymbol{E}_t = \frac{j\omega\mu_0}{k_c^2}\boldsymbol{e}_z \times \nabla_t H_z - \frac{j\beta}{k_c^2}\nabla_t E_z$$
$$\boldsymbol{H}_t = \frac{-j\omega\varepsilon_0}{k_c^2}\boldsymbol{e}_z \times \nabla_t E_z - \frac{j\beta}{k_c^2}\nabla_t H_z \tag{3.12}$$

where ∇_t is transverse gradient operator, ε_0 and μ_0 are the permittivity and permeability of vacuum, respectively. From (3.11)-(3.12), Transverse field components in cylindrical coordinate system are,

$$E_\rho = -j\frac{1}{k_c}\left[A_m\beta J_m^{'}(k_c\rho) + B_m\frac{k_0 m}{k_c\rho}J_m(k_c\rho)\right]\begin{Bmatrix}\cos(m\phi)\\ \sin(m\phi)\end{Bmatrix}$$

$$E_\phi = j\frac{1}{k_c}\left[A_m\frac{m\beta}{k_c\rho}J_m(k_c\rho) + B_m k_0 J_m^{'}(k_c\rho)\right]\begin{Bmatrix}\sin(m\phi)\\ -\cos(m\phi)\end{Bmatrix}$$

$$H_\rho = -j\frac{1}{\eta_0 k_c}\left[A_m\frac{k_0 m}{k_c\rho}J_m(k_c\rho) + B_m\beta J_m^{'}(k_c\rho)\right]\begin{Bmatrix}\sin(m\phi)\\ -\cos(m\phi)\end{Bmatrix} \qquad (3.13)$$

$$H_\phi = -j\frac{1}{\eta_0 k_c}\left[A_m k_0 J_m^{'}(k_c\rho) + B_m\frac{\beta m}{k_c\rho}J_m(k_c\rho)\right]\begin{Bmatrix}\cos(m\phi)\\ \sin(m\phi)\end{Bmatrix}$$

Boundary conditions (3.10) are then imposed to (3.13) and obtain,

$$\alpha - 1/\alpha = j\frac{k_c^2 a}{m\beta}\left(\frac{Z_\phi}{\eta_0} - \frac{\eta_0}{Z_z}\right)$$

(3.14)

where $\alpha = A_m/B_m$ is defined as a coupling coefficient connect E_z and H_z. Two solutions of (3.14) corresponds to hybrid modes *HE* (Re(α)>0) and *EH* (Re(α)<0), respectively. These are generalization of hybrid mode definition in corrugated waveguide [16]. Then dispersion relationship is deduced and can determine eigenvalue β and mode order n,

$$\left[\frac{J_m^{'}(k_c a)}{J_m(k_c a)} - j\frac{Z_\phi}{\eta_0}\frac{k_c}{k_0}\right]\left[\frac{J_m^{'}(k_c a)}{J_m(k_c a)} - j\frac{\eta_0}{Z_z}\frac{k_c}{k_0}\right] = \left(\frac{m\beta}{k_0 k_c a}\right)^2 \qquad (3.15)$$

Field components are then transformed into Cartesian coordinate system as follows:

$$E_x = j\frac{B_m}{k_c}\left[-\alpha\beta\begin{Bmatrix}\cos(m\phi)\cos\phi\\ \sin(m\phi)\cos\phi\end{Bmatrix}+k_0\begin{Bmatrix}-\sin\phi\sin(m\phi)\\ \sin\phi\cos(m\phi)\end{Bmatrix}\right]J_m^{'}(k_c\rho)$$
$$+j\frac{B_m}{k_c}\left[A_m\frac{m\beta}{k_c\rho}\begin{Bmatrix}-\sin\phi\sin(m\phi)\\ \sin\phi\cos(m\phi)\end{Bmatrix}-\frac{k_0 m}{k_c\rho}\begin{Bmatrix}\cos(m\phi)\cos\phi\\ \sin(m\phi)\cos\phi\end{Bmatrix}\right]J_m(k_c\rho)$$

$$E_y = j\frac{B_m}{k_c}\left[-\alpha\beta\begin{Bmatrix}\sin\phi\cos(m\phi)\\ \sin\phi\sin(m\phi)\end{Bmatrix}+k_0\begin{Bmatrix}\sin(m\phi)\cos\phi\\ -\cos(m\phi)\cos\phi\end{Bmatrix}\right]J_m^{'}(k_c\rho)$$
$$+j\frac{B_m}{k_c}\left[-\frac{k_0 m}{k_c\rho}\begin{Bmatrix}\sin\phi\cos(m\phi)\\ \sin\phi\sin(m\phi)\end{Bmatrix}+\frac{\alpha m\beta}{k_c\rho}\begin{Bmatrix}\sin(m\phi)\cos\phi\\ -\cos(m\phi)\cos\phi\end{Bmatrix}\right]J_m(k_c\rho)$$

(3.16)

When m=1, α=1 and use $\beta\approx k_0$ approximation for large aperture, E_x or E_y vanishes and the linear aperture field is ϕ-independent, which satisfy conditions (i') and (ii') in last part. From (3.14), when α=1, balanced hybrid boundary condition [12] holds

$$Z_\phi Z_z = \eta_0^2 \tag{3.17}$$

Therefore, a circular waveguide anisotropic surface satisfy (3.17) would support hybrid HE_{1n} that radiate low level crosspolar field theoretically. However, it is noticeable that EH_{1n} (α=-1) could also propagate in waveguide, which have equally E_x and E_y components and radiated high level crosspolar field. Fig. 3.4 illustrate dispersion curves for several cases under balance hybrid condition from (3.15). It shows in Fig. 3.4 (b), EH modes could be excited along with HE modes which is not desirable in high XPD communication application. From Fig. 3.4 (c), when $Z_\phi=0$ and $Z_z=\infty$,

waveguide could support single HE mode in a large bandwidth. This boundary condition can be realized by circumferentially corrugated wall with resonant slots which and will be stated in detail in next chapter. From Fig. 3.4 (b), surface with $Z_z = Z_\phi = j\eta_0$ is another possible choice for achieving the single balanced HE mode propagation over a large range of ka (bandwidth). In addition, cut-off for this mode is much lower than $Z_\phi = 0$ $Z_z = \infty$ case. This gives a potential that antenna with smaller aperture diameter could be used onboard for high XPD application. $Z_z = Z_\phi = j\eta_0$ may be can realized by artificial metamaterial technology.

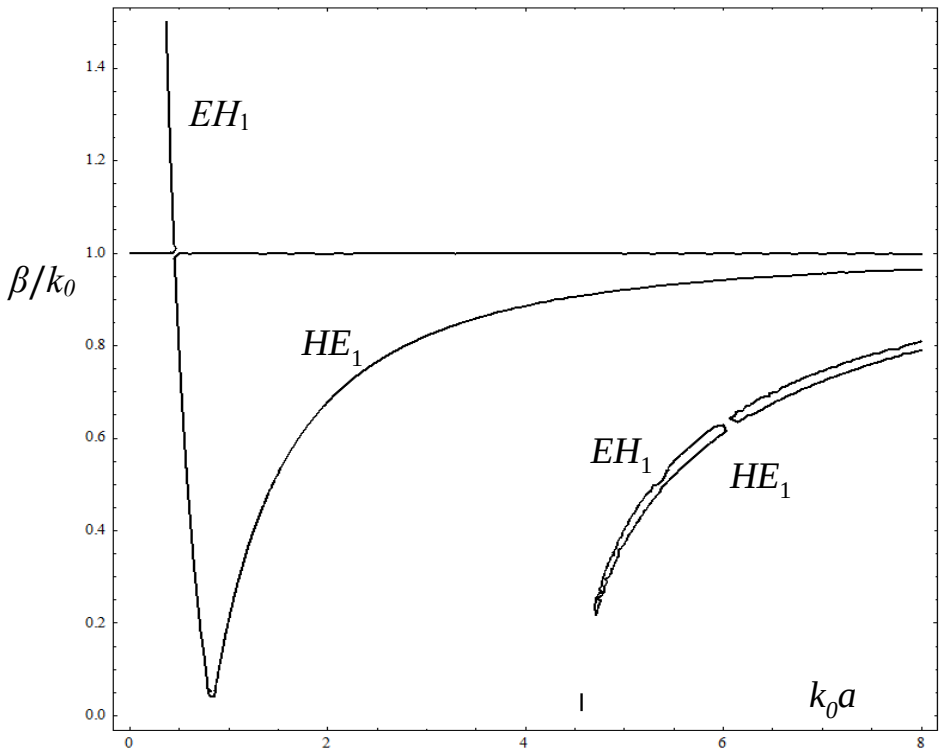

(a) $Z_z = Z_\phi = -j\eta_0$

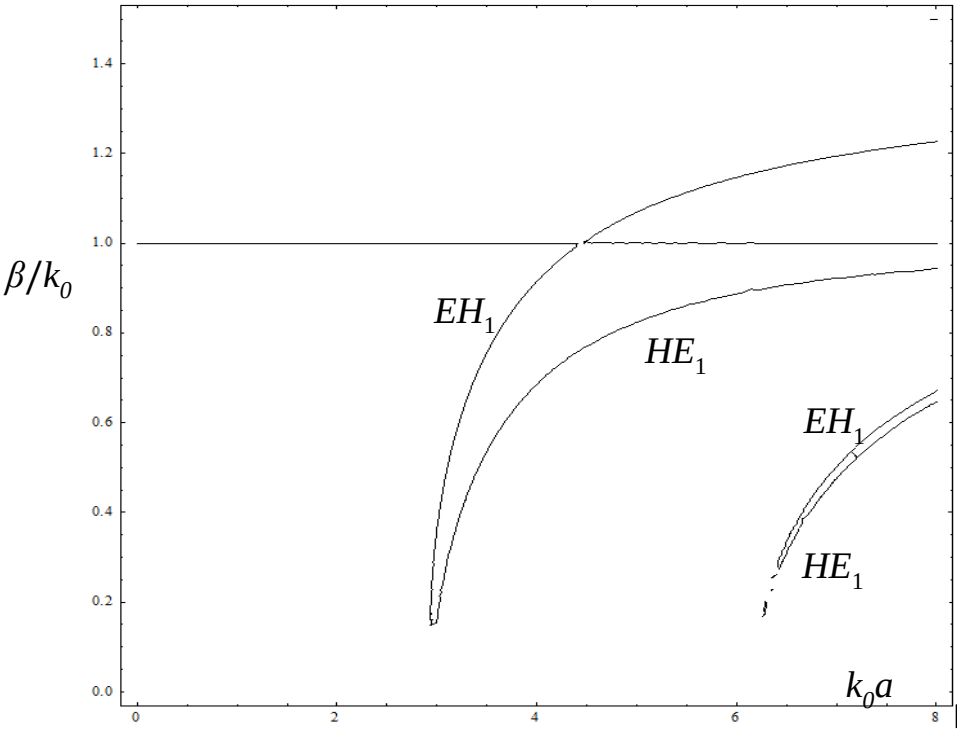

(b) $Z_z = Z_\phi = j\eta_0$

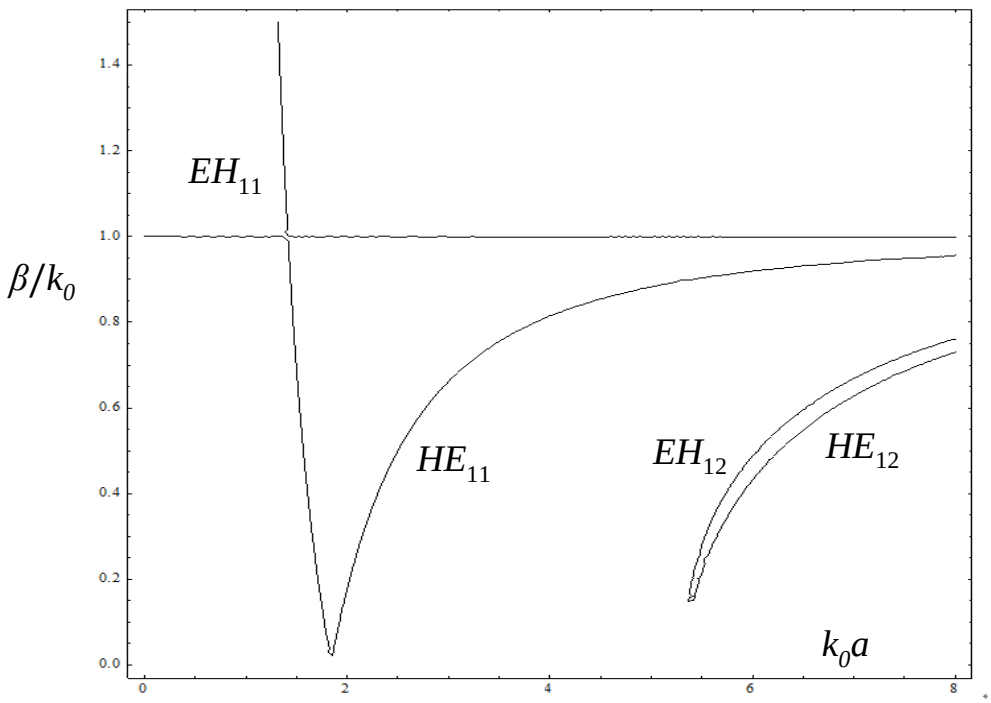

(c) $Z_\phi = 0$, $Z_z = \infty$

Fig.3.4. Dispersion curves under balance hybrid condition

4. Conical Corrugated Horn Antenna

Corrugated horn was first proposed for achieving symmetrical radiation patterns as feeds of reflector antenna. It was later realized that corrugated horns also radiate low-crosspolarization field and suitable for high XPD dual polarization application. It is nowadays widely used in various high restrictive applications [17] due to their good radiation performance, in particular their pattern symmetry and low crosspolarization.

4.1 Corrugated Surface and Waveguide

Corrugated waveguide is a special class of hybrid mode waveguide proposed in last chapter and the desired $Z_\phi = 0$ $Z_z = \infty$ surface can be approximately realized by corrugated surface. The structure of corrugated waveguide is shown in Fig. 4.1. According to [16], if there are enough corrugations per wavelength, the azimuthal electric field E_ϕ will be equal to zero at corrugation boundary $\rho = a$ and hence $Z_\phi = 0$. On the other hand, if the corrugation ridges are narrow and quarter wavelength deep ($d = \lambda_0/4$), they will act as short transmission lines where the short circuit at the end ($\rho = r_0$) is transferred to an open circuit at $\rho = a$. This makes that there will not be axial currents generated by H_ϕ, so $H_\phi = 0$ and then $Z_z = \infty$. Therefore, balanced hybrid condition is satisfied by quarter wavelength deep surface. Since $Z_z = \infty$ condition is wavelength dependent, balanced hybrid condition can only be fulfilled at a specific frequency.

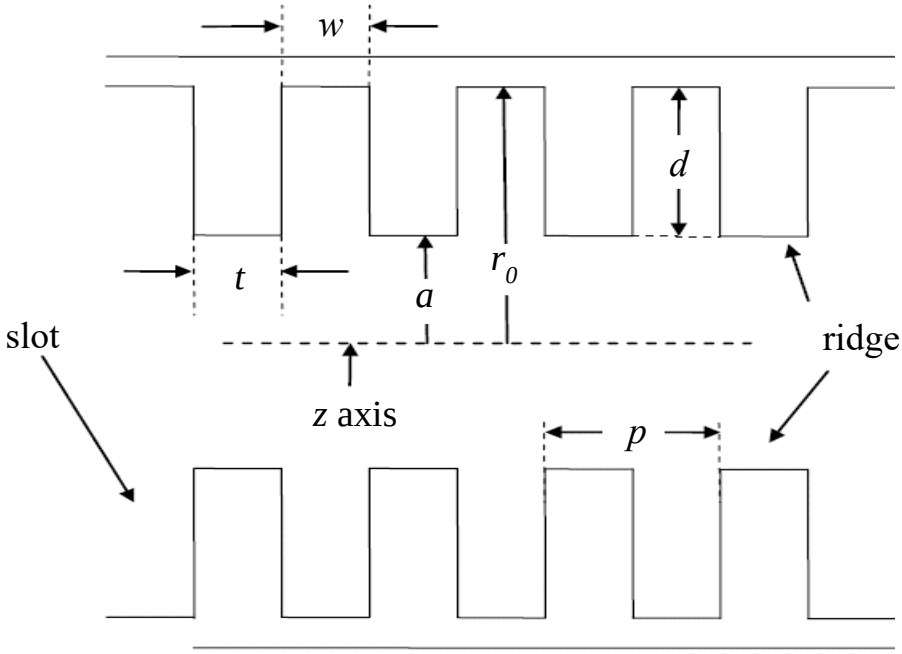

Fig. 4.1 Corrugated waveguide structure

When operating frequency deviate this specific frequency, $Z_\phi = 0$ but Z_z will be finite. From (3.14)-(3.16), aperture field of HE_{1n} modes is,

$$E_x = CJ_0(k_c\rho) + D\frac{\eta_0}{Z_z}\frac{1}{k_0 a}J_2(k_c\rho)\cos 2\phi$$

$$E_y = D\frac{\eta_0}{Z_z}\frac{1}{k_0 a}J_2(k_c\rho)\sin 2\phi$$

(4.2)

(4.12) explains why maximum cross polarization level appears in $\phi = \pm 45$ planes under LP operation.

Only m=1 modes are of interested as stated in last chapter. Under balanced hybrid condition with $\beta \approx k_0$ approximation, dispersion equation (3.15) reduces to

$$\frac{J_1'(k_c a)}{J_1(k_c a)} = \pm\left(\frac{1}{k_c a}\right) \tag{4.1}$$

Two sets of solutions of (4.1) are then obtained as

(1) $k_c a$ = zeros of $J_0(\cdot)$ = 2.405, 5.520, …correspond for HE_{1n} modes;

(2) $k_c a$ = zeros of $J_2(\cdot)$ = 5.136, …correspond for EH_{1n} modes

where HE_{1n} modes are linearly polarized and EH_{1n} modes have a high level crosspolar component. From Fig. 3.4 (c), in order not to excite EH modes waveguide, we hope waveguide support single-mode and excite purely dominant HE_{11} mode.

4.2 Conical Corrugated Horn Antenna as TE_{11} to HE_{11} Mode Converter

4.2.1 Principle of Conical Corrugated Horn

It has been stated from last chapter that the fundamental hybrid HE_{11} mode is approximately a combination of TE_{11} and TM_{11} modes in smooth circular waveguide modes with an appropriate relative phasing between them. The input aperture field distribution is usually the TE_{11} mode of a circular waveguide under single mode operation. Therefore, a TE_{11} to HE_{11} mode converter is necessary to generate desired HE_{11} mode in the output aperture. We use the normal conical corrugated horn antenna as a TE_{11} to HE_{11} converter. In a conventional smooth circular waveguide, the surface impedance is zero, i.e. Z_z =0. In a corrugated circular waveguide, Z_z is generally finite and has the value [18]

$$Z_z = \eta_0 \tan(k_0 d)\,(1-t/p) \tag{4.2}$$

From (4.2) it can be seen that slot depth $d=\lambda_0/2$ will lead to Z_z =0. Then

surface impedance in both smooth-walled and corrugated waveguides are matched. If $d=\lambda_0/4$ then balanced hybrid condition satisfied and thus $Z_z=\infty$. Hence if we change the depth of the slots from $\lambda_0/2$ to $\lambda_0/4$ smoothly over several periods, it gives possibility to excite a purely balanced HE_{11} mode and achieve impedance matching between smooth and corrugated structure.

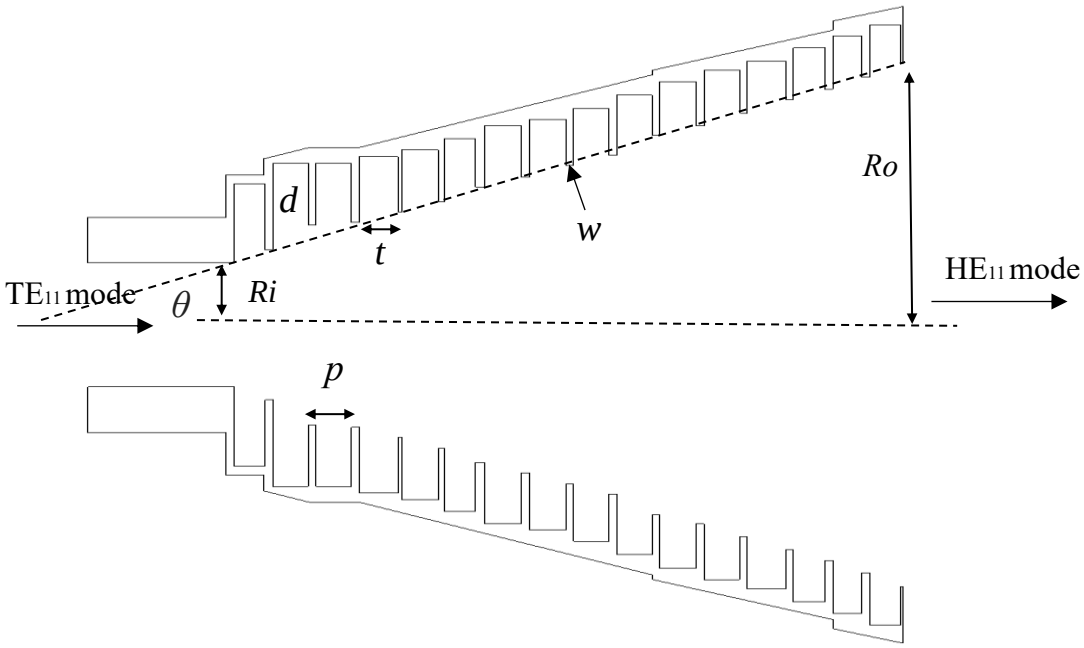

Fig.4.2 Conical Corrugated Horn Antenna with Design Parameter

4.2.2 Design Methodology and Simulation of Conical Corrugated Horn Antenna

Conical corrugated horn antenna with the design parameters are illustrated in Fig.4.2. Length of circular waveguide is chosen to > $\lambda_0/2$ to avoid mutual coupling between circular waveguide and polarizer. Design requirements are XPD>30dB and Gain>17dBi in operation X band (8.0GHz-8.4Ghz). All

parameters then will be designed at the center frequency 8.2GHz. Main parameters are considered by surface impedance model as follows:

(1) Input radius R_i

Ideally the input smooth circular waveguide should operate in single dominant TE_{11} mode over 8.0-8.4GHz. TE_{11} mode has the cutoff wavenumber $k_c=2\pi/\lambda_c=1.841/R_i$. Therefore, R_i must satisfy the inequality $2\pi R_i f_{min}/c \geq 1.841$, where $c=3\times10^8$ m/s is the speed of light. R_i is then chosen to be 13.6mm which makes circular matches septum polarizer output aperture well.

(2) Output radius R_o

According to relationship between directivity and aperture size for conical horn antenna, $4\pi\ (\pi\ R^2_o)/\ \lambda^2$-2.91(dBi) = Gain (dBi), R_o is chosen to be 57.6mm

(3) Period p and ridge width t

Period p is usually chosen to be satisfy $\lambda_c/10 \leq p \leq \lambda_c/5$, we choose p=6.0mm. From (4.2) it is shown ideally t/p should be as small as possible to achieve Z_z =0 over a larger bandwidth but this will cause difficulty in manufacturing. We choose t=1.0mm and t/p=0.83.

(4) Flare angle θ and horn length L

For onboard satellite application, antenna should be as compact as possible with larger θ when R_o is fixed. However, when θ become larger than 25

degree, surface impedance model become not accurate for perpendicular slots. We choose θ=25 $^{\circ}$, and L= (R_o- R_i) cot θ

(5) Corrugation depth d

Corrugation depths are chosen to be changing from from $\lambda_0/2$ to $\lambda_0/4$ smoothly. Antenna HFSS Simulation model are illustrated in Fig.4.3(a).

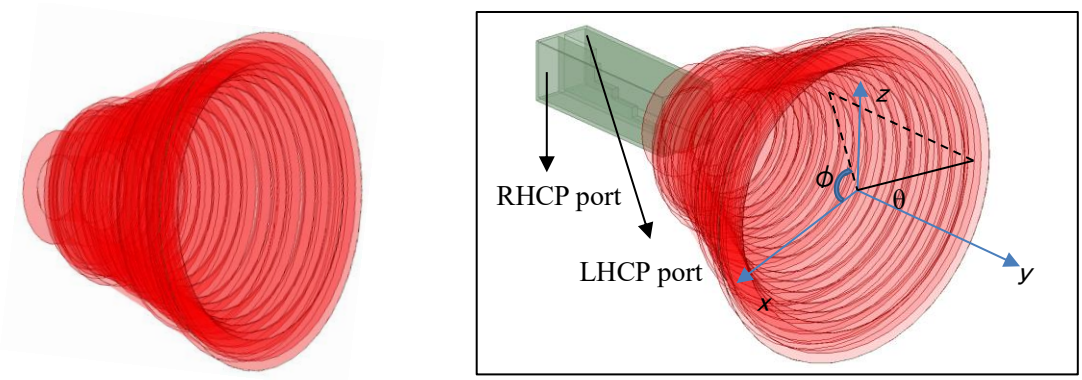

(a) Corrugated conical horn antenna (b) Complete antenna system

Fig.4.3. Simulation model

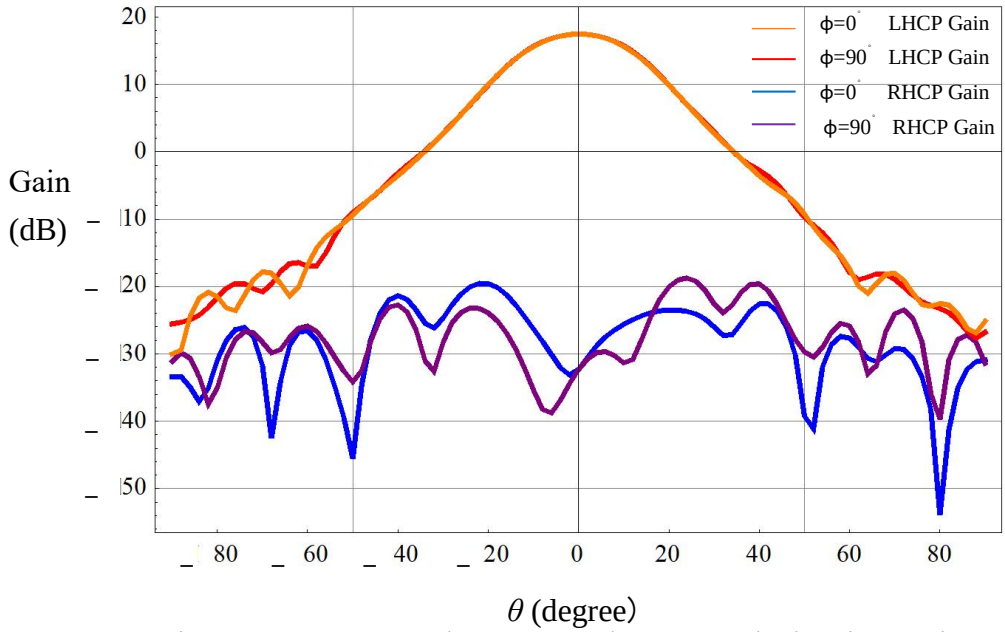

Fig.4.4 ϕ=0° ,90° plane co-and cross-polarization gain

Fig. 4.3 (b) shows the whole antenna system simulation model, we excite dominant mode in LHCP port of polarizer and get RHCP and LHCP radiation pattern at center frequency. XPD is then equal to G_{LHCP}[dBi]-G_{RHCP}[dBi]. Simulation results are given in Fig. 4.4-4.6 while Table. I show some representative values. It shows similar co-polarization φ=0° ,90° plane pattern and good XPD performance near boresight (θ=0°). We could obtain maximum XPD of 44dB and 17.6dBi co-polarization gain near the boresight over 400MHz bandwidth in X band (8-8.4GHz).

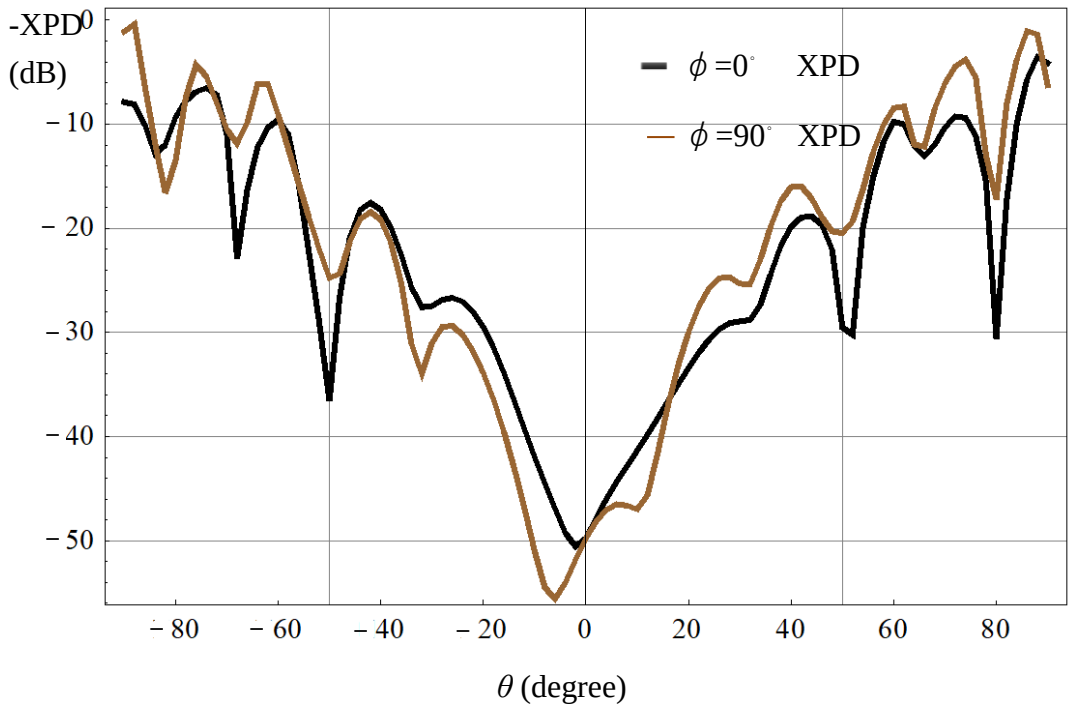

Fig.4.5 ϕ =0° ,90° plane XPD

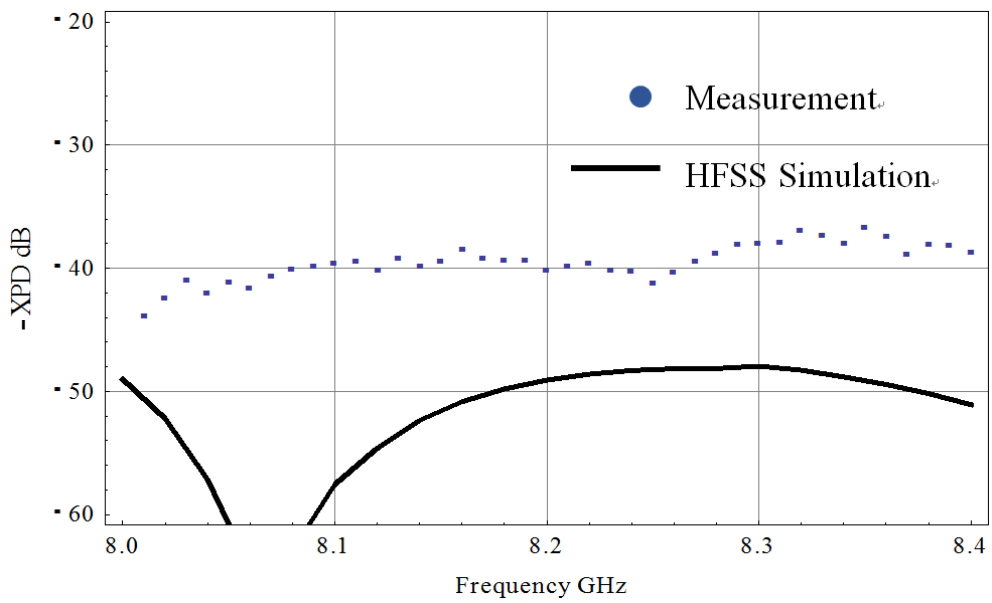

Fig.4.6 On-axis XPD versus frequency

Frequency [GHz]	Co-polarization gain [dBi]	XPD [dB]
8.0	17.20	43.23
8.2	17.30	40.30
8.4	17.60	38.92

TABLE.I. Representative value along boresight

However, it can also be observed from Fig.4.4-4.5 that off-axis XPD performance relatively not good. XPD>40dB can be achieved only in $-10^{\circ} \leq \theta \leq 10^{\circ}$ region.

5. Gaussian Corrugated Horn Antenna

5.1 Conceptual Idea

Although dominant HE_{11} mode propagate in hybrid waveguide (horn antenna) shows good linearity and circular symmetric, it is not stringent satisfies Huygens source condition and match the free space. It is well known in optic laser theory that gaussian beam modes are a solution of the paraxial wave equation in the free space and they form a basis of free space propagation. They are TEM mode, so Huygens source condition should be automatically satisfied. Some details about gaussian beam mode are stated in appendix.

Gaussian Profiled Horn Antennas (GPHA) were proposed to generate any kind of transverse field distribution with gaussian distributed features. Balanced HE_{11} mode has gaussian-like distribution. Hence if a GPHA is fed by HE_{11} mode wave, it is possible to excite high purity linearly distributed gaussian beam mode. Then it will naturally match waveguide and free space. This offer a possible method to obtain better XPD performance rather than HE_{11} mode. As in convention waveguide theory, usually only the fundamental gaussian TEM_{00} mode is of interest. Corrugated GPHA is proposed to obtain high purity TEM_{00} mode at output horn aperture [19]. If we could obtain horn aperture field distribution that is nearly the transverse field distribution of a fundamental TEM_{00} mode, its radiation pattern would be also nearly a fundamental gaussian beam propagation.

5.2 Design and Simulation Result

From Appendix A, *w(z)* is the beam radius which is the value of the radius at which the field decays 1/ *e* relative to its *z*-axis value, where $w_0=w(0)$ is beam waist. *w(z)* can be given by,

$$w(z) = w_0 \cdot \sqrt{1+\left(\frac{2z}{k_0 \cdot w_0^2}\right)^2} \tag{5.1}$$

The profile is designed to be same from as (5.1) to simulate gaussian beam broadening and propagation. Hence the corresponding inner corrugation profile would follows the curve is given by similar form:

$$R(z) = r_0 \cdot \sqrt{1+\left(\frac{2z}{k_0 \cdot w_0^2}\right)^2} \tag{5.2}$$

where r_0 is the input radius of the profile antenna. Assume $r_0=a \cdot w_0$, it is clear that this factor *a* would influence the flare angle of the horn antenna.

If a high purity HE_{11} mode feed the GPHA, after broaden, it should be expected that output is high purity gaussian beam mode due to the similarity between HE_{11} and TEM_{00} mode.

A conical corrugated horn excite high purity balanced HE_{11} is designed in last chapter and now used as a feed to corrugated GPHA. Thus r_0 is fixed as 57.6mm which is the radius of output conical antenna aperture. We choose *a*=0.65 for a compact structure. Corrugation size is designed same as conical horn. Simulation result shows that when gaussion profile length L >84mm it would not affect XPD performance much, so for compactness reason we choose L=84mm. Final GPHA system simulation model is shown in Fig.5.1. Simulation results are given in Fig. 5.2-5.3. It shows better XPD

performance near boresight (θ=0°) then conical corrugated horn antenna. We could obtain maximum XPD of 60dB and 20dBi co-polarization gain near the boresight at 8.2GHz. XPD>40dB can be achieved in -17° ≤θ≤17° region which better than conical corrugated antenna.

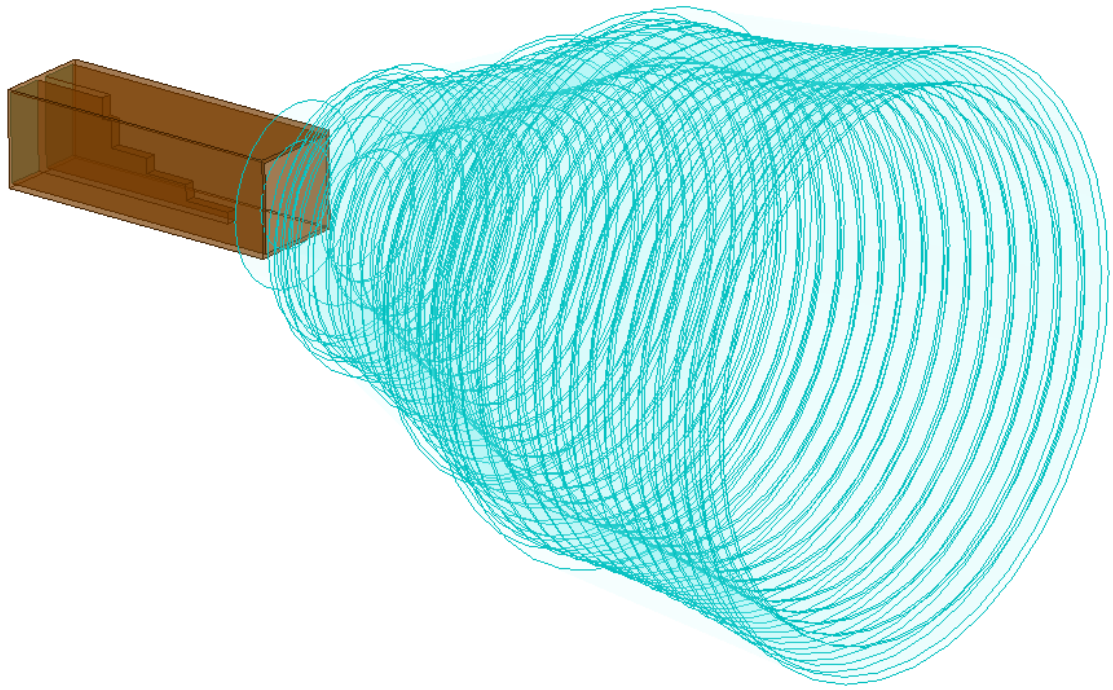

Fig.5.1. Gaussian Corrugated Horn Antenna with polarizer

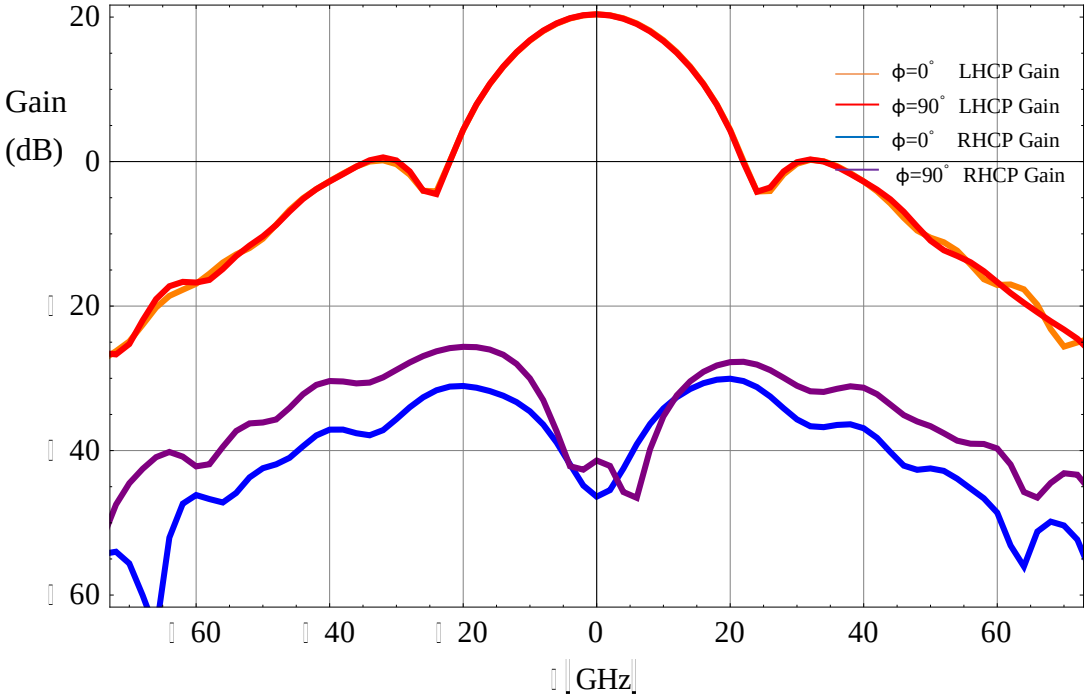

Fig.5.2. ϕ=0° ,90° plane co-and cross-polarization gain

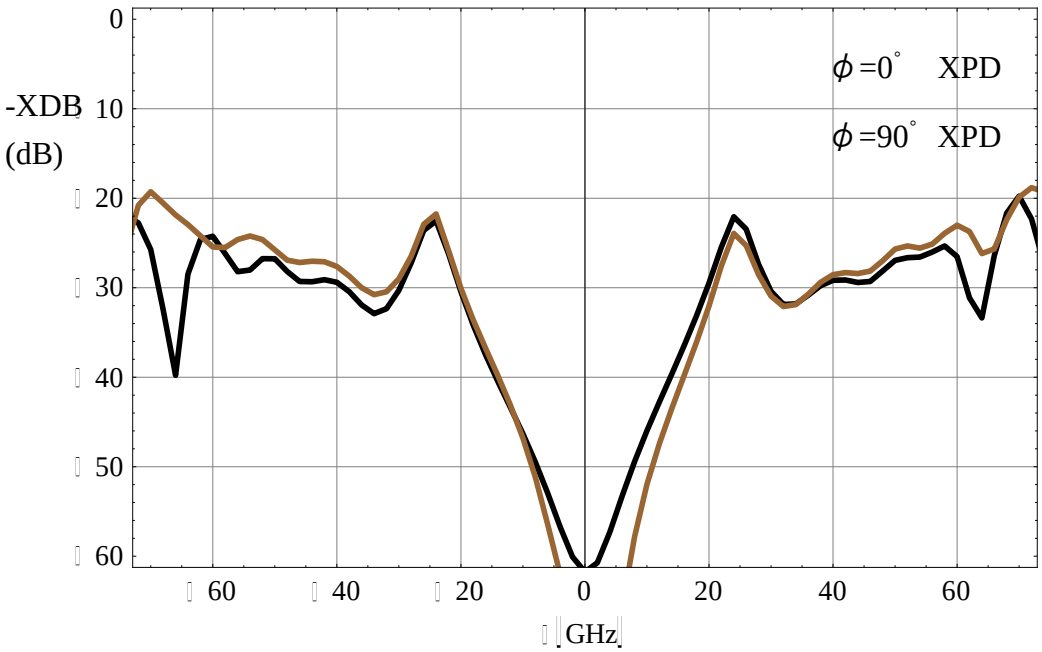

Fig.5.3. ϕ=0° ,90° plane XPD

6. Summary

High XPD performance of small satellite is important for achieving reliable high speed dual polarization communication. It is hard to improve off-axis XPD performance.

Aperture field conditions for high XPD dual CP is communication is derived by field equivalence principle. Hybrid mode circular waveguide with anisotropic surface impedance are analyzed in detail. Dispersion equation and electromagnetic field expressions are given analytically. It shows that HE_{1n} mode supported by waveguide satisfies balanced hybrid condition ideally radiate zero crosspolar field.

Corrugated surface with appropriate slot depth could satisfy balanced hybrid condition and achieve high XPD performance. Gaussian profiled technology combined with conventional corrugated horn technology shows possibility to further improve off-axis XPD performance.

Reference

[1] Hirobumi Saito, Edited by Henry Helvajian, “Small Satellites: Past, Present, and Future,” American Institute of Aeronautics and Astronautics (AIAA), pp. 449-485, 2009.

[2] Skybox Imaging, Inc., *LINK BUDGETS*, in Exhibit 43, SAT-LOA-20120322-00058, FCC, pp. 19-24, 2012.

[3] T. Fukami, et al, “Experiments of 505 Mbps Downlink with 64APSK Modulation from 50-kg Class Satellite,” 59th Symposium on Space Science and Technology, Kagoshima, 2015.

[4] T. Yasin, and R. Baktur, “Circularly polarized meshed patch antenna for small satellite application,” Antenna and Wireless Propagation Letters, IEEE, vol. 12, pp. 1057-1060, 2013.

[5] S. A. Hasan, “Design & measurement techniques for innovative, high performance, circularly polarized, ultra-wideband corrugated horn antenna with septum polarizer for space applications,” IEEE International Conference on Microwave Technology & Computational Electromagnetics (ICMTCE), 2011.

[6] C. Kumar, V.V. Srinivasan, V.K. Lakshmeesha, S. Pal, “Novel Dual Circularly Polarized Radiating Element for Spherical Phased Array Application,” IEEE Antennas and Wireless Propagation Letters, vol. 8, pp. 826-829, 2009.

[7] M. H. Chen and G. N. Tsandoulas, “A wide-band square-waveguide array polarizer,” IEEE Trans. Antennas Propagat., vol. AP-21, pp. 389–391, May

1973.

[8] 海田正大, “電波干渉計VSOP-2のための円偏波ポーラライザーの研究開発,” 大阪府立大学, 博士論文, 2009.

[9] E. J. Kowalski, D. S. Tax, M. A. Shapiro, J. R. Sirigiri, R. J. Temkin, T. S. Bigelow, D. A. Rasmussen, “Linearly polarized modes of a corrugated metallic waveguide,” IEEE Trans. Microw. Theory Tech., vol. 58, no. 11, pp. 2772-2780, Nov. 2010.

[10] S. P. Skobelev, P. S. Kildal, “A new type of the quasi-TEM eigenmodes in a rectangular waveguide with one corrugated hard wall,” Progress in Electromagnetics Research, vol. 102, pp. 143-57, 2010.

[11] S. P. Skobelev, P. S. Kildal, “Analysis of hard strip-loaded conical horn by the method of generalized scattering matrices,” IEEE Trans. Antennas Propag., vol. 51, no. 10, pp. 2918-2925, Oct. 2003.

[12] X. Ma, C. Huang, W. Pan, B. Zhao, J. Cui, and X. Luo, “A dual circularly polarized horn antenna in Ku-band based on chiral metamaterial,” IEEE Trans. Antennas Propag., vol. 62, no. 4, pp. 2307–2311, Apr. 2014.

[13] E. Lier, R. K. Shaw, “Design and simulation of metamaterial-based hybrid-mode horn antennas,” Electron. Lett., vol. 44, no. 25, pp. 1444-1445, Dec. 2008.

[14] H. C. Minnett, B. MacA. Thomas, “A method of synthesizing radiation patterns with axial symmetry,” IEEE Trans. Antennas Propag., vol. AP-14, pp. 654-656, Sep. 1966.

[15] S. J. Orfanidis, “Electromagnetic Waves and Antenna,” Piscataway,

Rutgers Univ. Press, 2004.

[16] P. J. B. Clarricoats, A. D. Olver, “Corrugated Horns for Microwave Antennas,” U.K., London: Peregrinus, 1984.

[17] J. Teniente, A. Martínez, B. Larumbe, A. Ibáñez, R. Gonzalo, “Design guidelines of horn antennas that combine horizontal and vertical corrugations for satellite communications,” IEEE Trans. Antennas Propag., vol. 63, no. 4, pp. 1314-1323, Apr. 2015.

[18] X. Zhang, “Design of Conical Corrugated Feed Horns for Wide-Band High-Frequency Applications,” Transactions on Microwave Theory and Techniques, Vol. 41, pp. 1263-1274, 1993.

[19] Del Río C., Gonzalo R. and Sorolla M., “High Purity Gaussian Beam Excitation by Optimal Horn Antenna”, Proc. Int. Symposium on Antennas and Propagation, Chiba, Japan, September 1996.

[20] P. F. Goldsmith, “Quasioptical Systems: Gaussian Beam Quasioptical Propagation and Applications,” New York, Wiley-IEEE Press, 1998.

Appendix A Fundamental Gaussian Beam Mode

Gaussian beams have been widely used and extensively analyzed in optic and laser theory. We are interested in gaussian beam modes in this thesis because gaussian modes are one of the commonly used mode family to describe free space radiation and satisfy Huygens source condition in Chapter 3. Paraxial approximation is needed for solving Maxwell equations to obtain the gaussian modes. This approximation is valid for horn antennas with moderate flare profiles. The paraxial approximation is shown as: The wave propagation or radiation can be expressed as a spatially concentrated beam (without much divergence, the angular divergence is less than about 30 degrees). This paraxial wave will be proved satisfying the paraxial Helmholtz equation. Gaussian beam modes will then be obtained as a complete set of solutions of paraxial Helmholtz equation. Detail derivations and expressions of gaussian beam mode in either rectangular or cylindrical coordinates could be found in reference [20]

A.1 Paraxial Wave Equation for Gaussian Beam

Assume angular temporal frequency is ω and time harmonic factor is $e^{j\omega t}$. ψ represents any component of electric field $\boldsymbol{E}$, of a wave propagating in free space. From electromagnetic wave theory, it is well known that ψ satisfies scalar Helmholtz equation:

$$\nabla^2\psi + k_0^2\psi = 0 \tag{1.1}$$

k_0 is free space wavenumber. For a plane wave, orientations of electric and magnetic fields are mutually perpendicular, and they both perpendicular to the propagation direction. Similar to the plane wave, for beam propagation it is still assumed that the electric field, magnetic field and propagation vector satisfy perpendicular condition. Assume wave propagates in z direction and have z-dependence factor e^{-jk_0z}. Hence electric field scalars can be written as:

$$E(x,y,z) = u(x,y,z)e^{-jk_0z} \tag{1.2}$$

where u is a complex function represents the non-plane wave part of the beam. Substitute (1.2) to (1.1),

$$\nabla_t^2 u + \frac{\partial^2 u}{\partial^2 z} - 2jk_0\frac{\partial u}{\partial z} = 0 \tag{1.3}$$

The paraxial approximation consists of:

(1) the variation along the direction of propagation of u is small over a distance comparable to a wavelength, i.e. $\frac{\partial^2 u}{\partial^2 z} << k_0\frac{\partial u}{\partial z}$;

(2) the z-direction variation of u is small compared to the variation in transverse direction (xy-plane), i.e. $\frac{\partial^2 u}{\partial^2 z} << \nabla_t^2 u$.

Therefore, the second term in (1.3) could be dropped and reduce to,

$$\nabla_t^2 u - 2jk_0\frac{\partial u}{\partial z} = 0 \tag{1.4}$$

which is the paraxial wave equation. Solutions to (1.4) are the Gaussian beam modes.

A.2 Fundamental Gaussian Beam Mode

A.2.1 Field Expression

The Gaussian beam modes are transverse electromagnetic (TEM) mode. The solution of paraxial Helmholtz equation (1.4) for the fundamental mode TEM_{00} (or HG_{00}, LG_{00}) can be expressed in cylindrical coordinate as:

$$u(\rho,\phi,z)=\frac{w_0}{w(z)}e^{\frac{-\rho^2}{w^2(z)}}\cdot e^{-j\frac{k_0\cdot\rho^2}{2R(z)}}\cdot e^{-j(k_0z-\xi(z))} \tag{1.5}$$

where normalization constant is neglected because it will not affect the mode shape. The free space propagation of the TEM_{00} mode is depicted in Figure A.1.

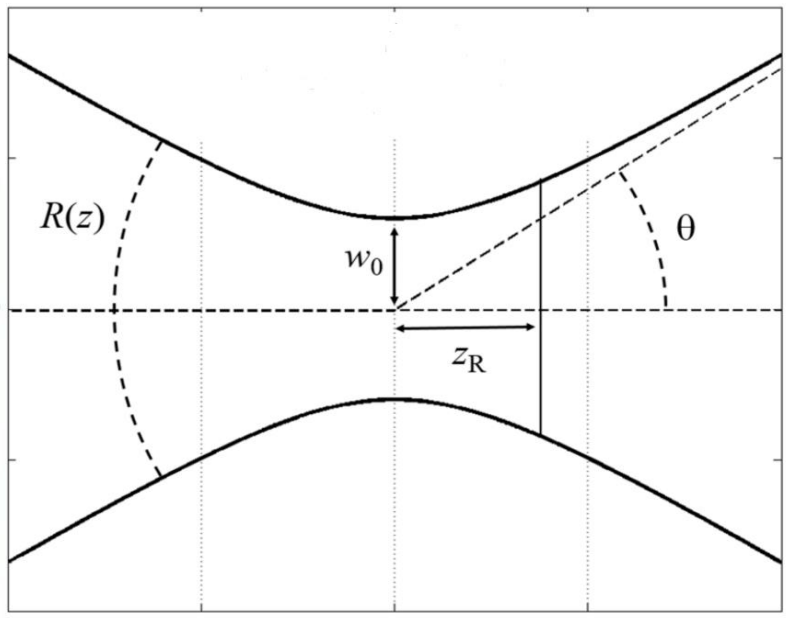

Fig A.1 Fundamental gaussian beam mode TEM_{00}

From (1.5), it can be observed that the fundamental TEM_{00} mode is ϕ

independent and circular symmetrical. The terms in (1.5) are explained as follows:

(1) $\rho = \sqrt{x^2 + y^2}$

(2) *w(z)* is the beam radius which is the value of the radius at which the field decays 1/ *e* relative to its *z*-axis value. w_0=*w*(0) is beam waist. *w(z)* can be given by,

$$w(z) = w_0 \cdot \sqrt{1 + \left(\frac{2z}{k_0 \cdot w_0^2} \right)^2} \tag{1.6}$$

Define another constant called the Rayleigh range z_R as $z_R = k_0\, w_0^2 / 2$, which is the distance from the waist where the beamwidth is exactly $w(z) = \sqrt{2} w_0$. Then (1.6) can be rewritten as,

$$w(z) = w_0 \cdot \sqrt{1 + \left(\frac{z}{z_R} \right)^2} \tag{1.7}$$

From (1.6), when $z \gg z_R$ the beam radius expands linearly as $w(z) \approx w_0\, z/z_R$. The divergence angle of the TEM_{00} mode is defined as,

$$\theta_0 = \arctan(w_0 / z_R) \tag{1.8}$$

A reduction in either beam waist w_0 or frequency will cause an increase of beam divergence.

(3) *R*(*z*) is the radius of curvature of the beam's wavefront at *z*, and it is defined by,

$$R(z) = z \cdot \left[1 + \left(\frac{z_R}{z} \right)^2 \right] \tag{1.9}$$

The variation of *R*(*z*) versus z is depicted in Fig A.2. It is shown that *R*(*z*)

decreases from planar wave fronts at the beam waist ($R(z)=\infty$) to its minimum value at z_0.

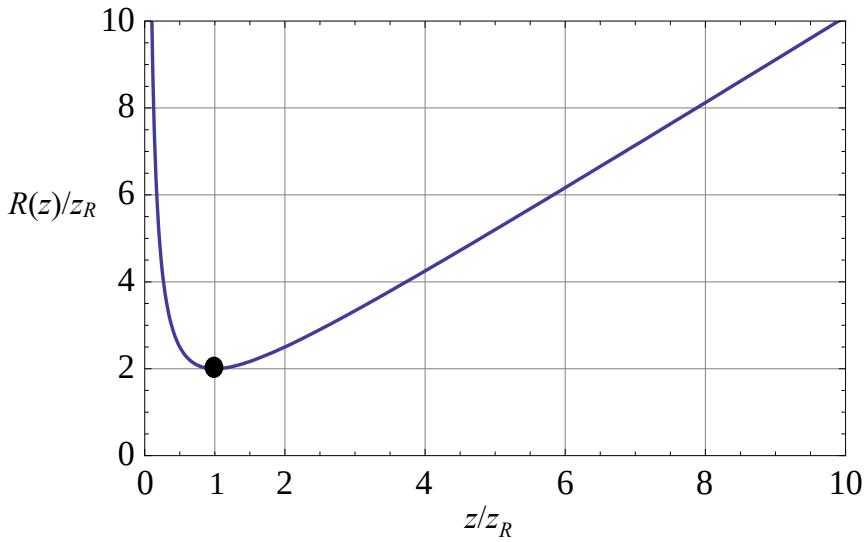

Fig A.2 Wavefront radius of curvature $R(z)$ versus z

(4) $\xi(z)$ is called the Gouy phase of the beam and expressed by

$$\xi(z) = \arctan(z / z_R)$$

Assume that electric field is linearly polarized in x direction. From (1.2) and (1.5), electric field is given by:

$$\boldsymbol{E}(\rho,\phi,z) = \boldsymbol{e}_x E_0 \frac{w_0}{w(z)} e^{\frac{-\rho^2}{w^2(z)}} \cdot e^{-j\frac{k_0 \cdot \rho^2}{2R(z)}} \cdot e^{-j(k_0 z - \xi(z))} \tag{1.10}$$

Then associated magnetic field oriented in y direction and can be calculated by

$$\boldsymbol{H}(\rho,\phi,z) = \boldsymbol{e}_y \frac{1}{\eta_0} E_x(\rho,\phi,z) \tag{1.11}$$

A.2.2 Intensity and Power

The intensity distribution can then be found by evaluating the Poynting vector from (1.10) and (1.11),

$$I(\rho,z)=\frac{\mathrm{Re}(\boldsymbol{E}\times\boldsymbol{H}^{*})}{2}=\frac{\left|\boldsymbol{E}(\rho,z)\right|^{2}}{2\eta_{0}}=I_{0}\left(\frac{w_{0}}{w(z)}\right)^{2}e^{\frac{-2\rho^{2}}{w^{2}(z)}} \tag{1.12}$$

where $I_0=\left|E_0\right|^2/2\eta_0$ is the intensity at the center of beam waist. The TEM_{00} field intensity distribution at any fixed z position is illustrated in Fig A.3. Fig A.4 depicts normalized intensity at different z position. It can be observed how the beam intensity shape diminishes and broadens while propagating in z axis. It can be observed the intensity decays half of its value at the beam waist a $z=z_0$.

The total power carried by a TEM_{00} mode beam can be derived by,

$$P_0=\int_0^{2\pi}\int_0^{\infty}I(\rho,z)\rho d\rho d\phi=2\pi\int_0^{\infty}I(\rho,z)\rho d\rho=\frac{1}{2}I_0(\pi\cdot w_0^2) \tag{1.13}$$

The power P carried within the circle of radius r_0 in the transverse plane at a certain z position is,

$$P=2\pi\int_0^{r_0}I(\rho,z)\rho d\rho=P_0(1-e^{\frac{-2r_0^2}{w^2(z)}}) \tag{1.14}$$

Therefore, the power transmits in a circular aperture of radius $r_0=w(z)$ is about $1-e^{-2}=86.5\%$ of the total power P_0. Similarly, within radius of $r_0=1.5w(z)$ approximately *98.9%* of the total power P_0 is concentrated.

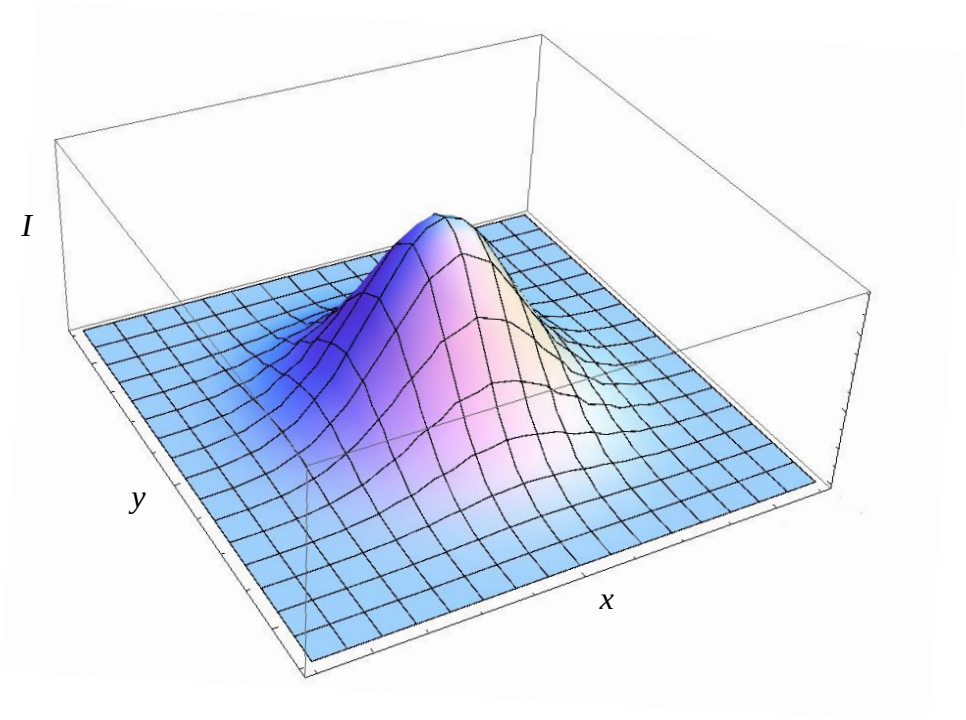

Fig A.3 3D distribution of TEM_{00} mode intensity at a fixed z

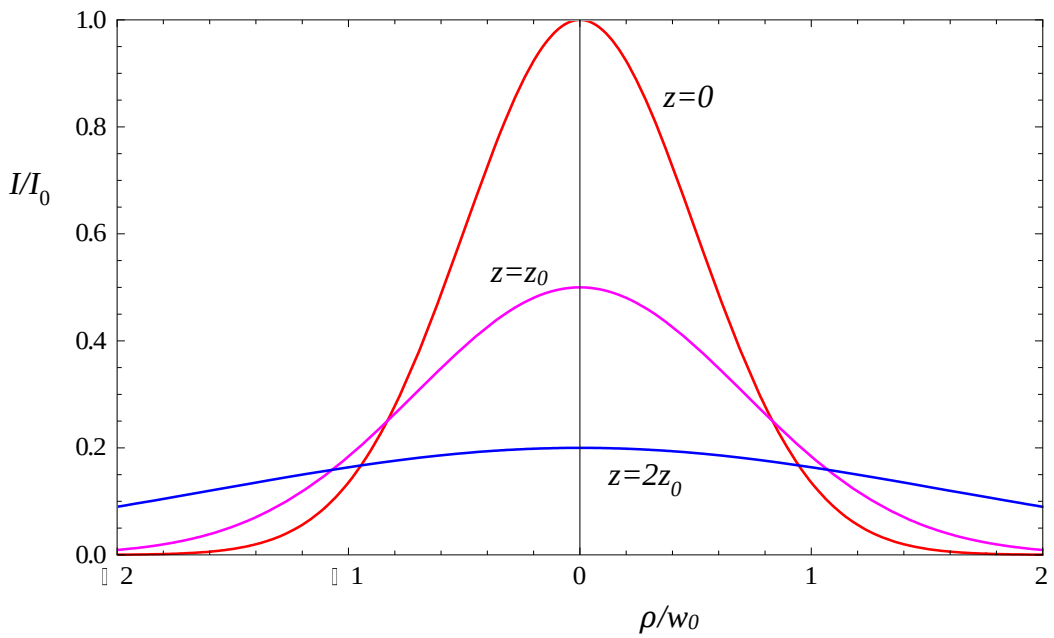

Fig A.4 TEM_{00} mode normalized intensity distribution at different z

学会発表

[1] Wang Tianyu，Hirobumi Saito, “Theory of Hybrid Mode Waveguide for High XPD Dual Circular Polarization Communication,” 電子情報通信学会宇宙・航行エレクトロニクス研究会, SANE, 2018 年 7 月